Theoretical Study on the Photophysical Properties of Hexapyrrolidine C_{60} Adducts with T_h, D_3, and S_6 Symmetries

X.-D. Li,[†] W.-D. Cheng,*[,†,‡] D.-S. Wu,[†,‡] Y.-Z. Lan,[†] H. Zhang,[†] Y.-J. Gong,[‡] F.-F. Li,[‡] and J. Shen[‡]

Fujian Institute of Research on the Structure of Matter, Chinese Academy of Sciences, State Key Laboratory of Structural Chemistry and Laboratory of Materials Chemistry and Physics, Fuzhou, Fujian 350002, People's Republic of China

Received: October 10, 2004; In Final Form: January 25, 2005

The equilibrium geometries of three isomeric hexapyrrolidine C_{60} adducts with T_h, D_3, and S_6 symmetries are optimized by means of the B3LYP method at the 6-31G* basis sets in this paper. On the basis of the optimized structures, the excited state and third-order nonlinear optical properties, such as third-harmonic generation (THG), electric-field-induced second-harmonic generation (EFISHG), and degenerate four-wave mixing (DFWM), and two-photon absorption (TPA) cross sections, δ, are calculated by using the TDB3LYP model based on the 6-31G* level coupled with the sum-over-states (SOS) method. The computational results show that the transition energies from S_0 to S_1 of the T_h hexaadduct and the D_3 hexaadduct have a remarkable blue shift by comparison with that of the C_{60} parent. These results are in agreement with experimental ones. However, the first singlet excitation energy of the S_6 hexaadduct has a red shift compared with that of the C_{60} parent. Accordingly, we predict that different positions located by six addends may result in the different spectrum properties. Finally, the two-photon absorption cross sections indicate that the largest average value of resonant TPA, $\langle\delta\rangle$, of the D_3 hexaadduct has a red shift compared with those of the T_h and S_6 hexaadducts.

I. Introduction

Since the discovery and the beginning of the large-scale production of fullerenes, many efforts have been made to study the physical and chemical properties of these novel molecules. Recently, increasing interest has been paid to the investigation on the photophysical properties of the functionalized derivatives of fullerene C_{60},[1−8] which have shown potential applications in various fields. From the previous investigations on fullerene C_{60} derivatives, it has been found that most [6,6]-closed C_{60} derivatives have similar absorption spectra and fluorescence spectra, with a maximum wavelength absorption peak at ∼690 nm and a fluorescent peak at ∼710 nm. However, the hexapyrrolidine fullerene C_{60} derivatives with T_h and D_3 symmetries show a remarkable fluorescence peak at ∼540 nm, which was reported by Schick et al. in 1999.[9] At the same time, one of these C_{60} adducts, T_h hexapyrrolidine (THP),[10] has been utilized as a chromophore in the fabrication of a white light organic light-emitting diode (LED) for its unusual photophysical properties. To determine how the functionalized groups affect the photophysical properties of the native C_{60} cage, we select three isomeric hexapyrrolidine C_{60} derivatives $C_{72}H_{30}N_6$ with different symmetries as the investigation subject of this paper. The equilibrium geometries and excited state properties will be calculated on the basis of the ab initio methods with Gaussian98 programs for these C_{60} derivatives.

Third-order nonlinear optical (NLO) properties provide the basic means for controlling light with light (all optics), as in optical bistablility and phase conjugation. Furthermore, the realization of all-optical switching, modulating, and computing devices is an important goal in modern optical technology, and NLO materials with large third-order nonlinear susceptibilities are indispensable for such devices. Accordingly, frequency-dependent third-order NLO polarizabilities and two-photon absorption (TPA) cross sections of hexapyrrolidine C_{60} adducts with different symmetries have been calculated by using the time-dependent density functional theory (TDDFT) model combined with the sum-over-states (SOS) method in this paper.

II. Computational Procedures

Using the ab initio density functional theory (DFT) model of the GAUSSIAN98 program,[11] the geometrical optimization of three hexapyrrolidine C_{60} derivatives are carried out with the B3LYP[12] method at the 6-31G* level. The input initial structures of the three species are constructed from the geometrical structure of functionalized group and optimized C_{60} framework. In addition, symmetry constraint has been applied in the process of optimization. According to the C6−C6 double bond position located by six addends,[13] we construct three hexapyrrolidine C_{60} derivatives with T_h, D_3, and D_{3d} (S_6) symmetries, respectively. When six addends locate only in *e* and *trans*-1 position, the T_h hexaadduct (Figure 1a) can be built. The D_3 hexaadduct (Figure 1b) has its six addends either in *e*, *cis*-2, *trans*-1, *trans*-2, or *trans*-3 relationships, whereas the D_{3d} (S_6) hexaadduct (Figure 1c) has *trans*-1, *trans*-4, and *cis*-3 relationships. Figure 1 presents the optimized geometrical structures of these compounds.

To interpret the photophysical properties of these hexapyrrolidine fullerene C_{60} derivatives, we employ the time-dependent density functional theory (TDDFT) model[14−16] with the B3LYP method at the 6-31G* basis set to calculate the transition energies and oscillator strengths, respectively. Here, the B3LYP designs Becke three parameter of Lee−Yang−Parr hybrid

[†] State Key Laboratory of Structural Chemistry.
[‡] Laboratory of Materials Chemistry and Physics.

10.1021/jp045377w CCC: $30.25
Published on Web 03/09/2005

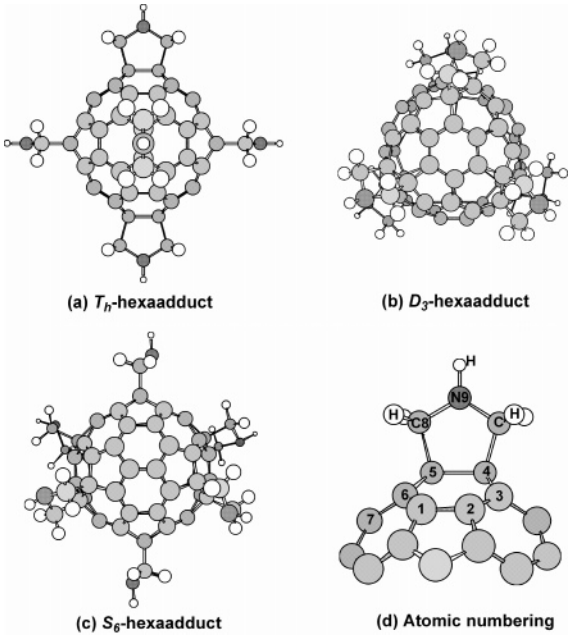

Figure 1. Optimized geometrical configurations of hexapyrrolidine C_{60} adducts $C_{72}H_{30}N_6$ and atomic numbering.

functions including exact exchange and the correlation functions. Then, their frequency-dependent third-order NLO polarizabilities have been calculated by using the sum-over-states (SOS) method.[17,18] The expression of third-order polarizability, γ, is obtained by application of time-dependent perturbation theory to the interacting electromagnetic field and microscopic system.[17,18] Straightforward application of standard quantum mechanical time-dependent perturbation theory, however, leads to unphysical secular divergences in $\gamma_{abcd}(-\omega_p; \omega_1, \omega_2, \omega_3)$ when any subset of the frequencies ω_1, ω_2, and ω_3 sums to zero. Fortunately, the divergences are eliminated by employing a damping factor, $i\Gamma$,[19] as described in the following.

$$\gamma_{abcd}(-\omega_p; \omega_1, \omega_2, \omega_3) = \left(\frac{2\pi}{h}\right)^3 K(-\omega_p; \omega_1, \omega_2, \omega_3)e^4 \times \left\{ \sum_P \left[\sum_{i,j,k}{}' \frac{\langle o|r_a|k\rangle\langle k|r_b^*|j\rangle\langle j|r_c^*|i\rangle\langle i|r_d|o\rangle}{(\omega_{ko} - \omega_p - i\Gamma_{ko})(\omega_{jo} - \omega_1 - \omega_2 - i\Gamma_{jo})(\omega_{io} - \omega_1 - i\Gamma_{io})} \right] - \sum_P \left[\sum_{j,k}{}' \frac{\langle o|r_a|j\rangle\langle j|r_b|o\rangle\langle o|r_c|k\rangle\langle k|r_d|o\rangle}{(\omega_{jo} - \omega_p - i\Gamma_{jo})(\omega_{jo} - \omega_1 - i\Gamma_{jo})(\omega_{ko} + \omega_2 + i\Gamma_{ko})} \right] \right\} \quad (1)$$

Here, $\langle o|r_a|k\rangle$ is an electronic transition moment along the a axis of the Cartesian system, between the reference state $\langle o|$ and the excited state $\langle k|$; $\langle k|r_b^*|j\rangle$ denotes the dipole difference operator equal to $[\langle k|r_b|j\rangle - \langle o|r_b|o\rangle\delta_{kj}]$; and $h\omega_{ko}$ is the energy difference between state k and reference state o. The transition moments and dipole moments can be obtained from the calculated results on the basis of the TDB3LYP model. ω_1, ω_2, and ω_3 are the frequencies of the perturbating radiation fields, and $\omega_p = \omega_1 + \omega_2 + \omega_3$ is the polarization response frequency.Σ_P indicates an average over all permutations of ω_p, ω_1, ω_2, and ω_3 along with associated indices a, b, c, and d; Σ' indicates a sum over all states but reference state o. The factor $K(-\omega_p; \omega_1, \omega_2, \omega_3)$ accounts for distinguishable permutations of the input frequencies, and its value is given by $2^{-m}D$, where m is the number of nonzero input frequencies minus the number of nonzero output frequencies and D is the number of distinguishable orderings of the set $\{\omega_1, \omega_2, \omega_3\}$. As specific examples, for third-harmonic generation (THG), $K(-3\omega; \omega, \omega, \omega) = {}^1/_4$; for electric-field-induced second-harmonic generation (EFISHG), $K(-2\omega; \omega, \omega, 0) = {}^6/_4$; and for degenerate four-wave mixing (DFWM), $K(-\omega; \omega, \omega, -\omega) = {}^3/_4$. Accordingly, when input and output frequencies are all zero, that is, the static case, $K(0; 0, 0, 0) = 1$ for the THG, EFISHG, and DFWM optical processes. In practical calculations, if ω_1, ω_2, and ω_3 (as well as their arbitrary linear combinations) can be chosen to be away from a resonant frequency, all of the damping factors, $i\Gamma$, can be neglected and eq 1 will be reduced as eq 2.

$$\gamma_{abcd}(-\omega_p; \omega_1, \omega_2, \omega_3) = \left(\frac{2\pi}{h}\right)^3 K(-\omega_p; \omega_1, \omega_2, \omega_3)e^4 \times \left\{ \sum_P \left[\sum_{i,j,k}{}' \frac{\langle o|r_a|k\rangle\langle k|r_b^*|j\rangle\langle j|r_c^*|i\rangle\langle i|r_d|o\rangle}{(\omega_{ko} - \omega_p)(\omega_{jo} - \omega_1 - \omega_2)(\omega_{io} - \omega_1)} \right] - \sum_P \left[\sum_{j,k}{}' \frac{\langle o|r_a|j\rangle\langle j|r_b|o\rangle\langle o|r_c|k\rangle\langle k|r_d|o\rangle}{(\omega_{jo} - \omega_p)(\omega_{jo} - \omega_1)(\omega_{ko} + \omega_2)} \right] \right\} \quad (2)$$

In this way, although the damping factors are not included in eq 2, the resonant divergences will be able to avoid and the nonresonant third-order polarizability tensor, γ, can be calculated. Throughout the paper, the symbols $\gamma(3\omega)$, $\gamma(2\omega)$, and $\gamma(\omega)$ represent the third-order polarizability of THG $\gamma(-3\omega; \omega, \omega, \omega)$, EDISHG $\gamma(-2\omega; \omega, \omega, 0)$, and DFWM $\gamma(-\omega; \omega, \omega, -\omega,)$, respectively. The prefactor $K(-\omega_p; \omega_1, \omega_2, \omega_3)$ is the relative magnitude of the reference state nonlinear polarizabilities for each optical process at nonzero frequency. In the following calculations, we use the same prefactor K in order to make the remark to justify plotting curves for the nonlinear polarizabilities of three optical processes against common axes. In eqs 1 and 2, the first summation involves the two-photon allowed states, which is referred to the type-II terms, and the second summation involves the one-photon allowed states, which is referred to the type-I terms.

The frequency dependence of TPA cross section, $\delta(\omega)$, is related to the imaginary part of the third-order polarizability in the DFWM optical process, $Im\gamma(-\omega; \omega, \omega, -\omega)$ by[20]

$$\delta(\omega) = \frac{32\pi^4\hbar}{n^2\lambda^2} L^4 Im\gamma(-\omega; \omega, \omega, -\omega) \quad (3)$$

where n is the index of refraction of the medium (vacuum assumed for the calculations) and L is a local field factor (equal to 1 for vacuum). Because the calculations of $\delta(\omega)$ only involve the two-photon states, the third-order polarizability of two-

photon resonance enhancement in degenerate four-wave mixingleaves only behind the first term (type II) and can be written as

$$\gamma_{abcd}(-\omega;\omega,\omega,-\omega) = \frac{3}{4}\left(\frac{2\pi}{h}\right)^3 e^4 \times \sum_j{}'(\omega_{jo} - 2\omega - i\Gamma_{jo})^{-1} \left[\sum_k{}'\frac{(\langle o|r_a|k\rangle\langle k|r_b^*|j\rangle + \langle o|r_b|k\rangle\langle k|r_a^*|j\rangle)}{(\omega_{ko} - \omega)} \times \sum_i{}'\frac{(\langle j|r_c^*|i\rangle\langle i|r_d|o\rangle + \langle j|r_d^*|i\rangle\langle i|r_c|o\rangle)}{(\omega_{io} - \omega)}\right] \quad (4)$$

Then, we take out the imaginary part $Im\gamma$ of this formula, and $\langle Im\gamma\rangle = {}^1/_5(Im\gamma_{xxxx} + Im\gamma_{yyyy} + Im\gamma_{zzzz} + Im\gamma_{xxyy} + Im\gamma_{xxzz} + Im\gamma_{yyxx} + Im\gamma_{yyzz} + Im\gamma_{zzxx} + Im\gamma_{zzyy})$. Here, the state $|j\rangle$ is a two-photon resonance state for which $\omega_{jo} - 2\omega = 0$ in the range over which ω is scanned in the calculation or experiment. Γ_{jo} is the damping factor, and we have assumed a constant parameter of $h\Gamma = 0.01$ eV in our work. Finally, in the calculations of third-order nonlinear optical properties, we only concern ourselves with the contributions from electric dipole transitions because they are the most intense as compared with vibrational and rotational transitions.[21]

III. Results and Discussions

(1) Geometrical Structures of the Hexapyrrolidine Fullerene C_{60} Derivatives. Parts a−c of Figure 1 present the optimized geometrical structures of the T_h, D_3, and S_6 hexaadducts, and Figure 1d illustrates the part of the functionalized group connecting with the C_{60} parent. In addition, we can obviously find the constituent elements of functionalized groups and their corresponding atomic numbering in Figure 1d.

In the T_h hexaadduct, it can be found that the geometrical parameters in the vicinity of the functionalized group have remarkable changes by comparison with the ones of the parent C_{60} calculated by the B3LYP method at the 6-31G* level.[22] The bond lengths of C4−C5 and C5−C6 are 1.611 and 1.534 Å, respectively, which are 0.216 and 0.080 Å, respectively, larger than that of the parent C_{60}. The angle of C4−C5−C6 decreases by 5.6° from 120.0° of the parent C_{60} to 114.4°, whereas the angle of C5−C6−C7 increases from 108.0 to 110.8°. Another large change is that the coplanar properties in hexagon and pentagon rings disappear after the addition of the functionalized group. The dihedral angles of C1−C2−C3−C4 and C2−C3−C4−C5 are 12.7 and −12.0°, respectively. Moreover, a noticeable characteristic is that the pentagon rings of the functionalized group have a planar property.

For the D_3 hexaadduct, the similar geometrical parameters can be found in Table 1. The bond lengths of C4−C5 and C5−C6 are 1.617 and 1.533 Å, respectively, which are 0.222 and 0.079 Å, respectively, larger than that of the parent C_{60}. The angle of C4−C5−C6 decreases by 5.3° from 120.0° of the parent C_{60} to 114.7°, whereas the angle of C5−C6−C7 increases from 108.0 to 110.9°. The remarkable difference from the T_h hexaadduct is that the dihedral angle of C4−C5−C8−N9 is 27.6°, where that of the T_h hexaadduct is 0.0°. That is to say, the pentagon rings of the functionalized group in the D_3 hexaadduct have no planar property.

TABLE 1: Some Geometrical Parameters of the T_h, D_3, and S_6 Hexaadducts Calculated by the B3LYP Method at the 6-31G* Level (the Data in Parentheses Are Experimental Values)

		T_h	D_3	S_6
bond lengths (Å)	C_4-C_5	1.611 (1.606)	1.617 (1.603)	1.611
	C_5-C_6	1.534 (1.522)	1.529 (1.533)	1.528
	C_6-C_7	1.424 (1.414)	1.424 (1.428)	1.420
	C_5-C_8	1.572 (1.595)	1.561 (1.577)	1.560
	C_8-N_9	1.433 (1.472)	1.457 (1.466)	1.458
bond angles (deg)	$C_4-C_5-C_6$	114.4 (114.3)	114.7 (112.4)	113.9
	$C_5-C_6-C_7$	110.8 (111.3)	110.3 (110.5)	110.4
	$C_6-C_5-C_8$	111.7 (111.7)	113.6 (111.4)	112.2
	$C_5-C_8-N_9$	105.7 (104.6)	103.3 (104.9)	105.6
dihedral angles (deg)	$C_1-C_2-C_3-C_4$	12.7 (12.5)	12.6 (14.6)	13.2
	$C_2-C_3-C_4-C_5$	−12.0 (−12.0)	−11.9 (−12.7)	−10.3
	$C_4-C_5-C_8-N_9$	0.0 (20.1)	27.6 (20.7)	27.9
	$C_6-C_5-C_8-N_9$	124.8 (145.5)	151.8 (144.5)	151.6

In the D_{3d} hexaadduct, the pentagon rings of the functionalized group have a planar property. However, when the nitrogen atoms deviate from the plane of functionalized group rings, the energy will be significantly decreased. At the same time, the symmetry reduces from D_{3d} to S_6. The calculated results at the B3LYP/6-31G* level indicate that the energy of the S_6 hexaadduct is lower by 48.5 kcal/mol than that of the D_{3d} hexaadduct. The lower energy of the S_6 hexaadduct may be ascribed to small steric effects between the neighboring functionalized groups, which makes the S_6 structure energetically favorable. In view of this result, the photophysical properties of the S_6 hexaadduct will be discussed in a later section.

Table 1 lists some optimized geometrical parameters of the S_6 hexaadduct. It can be obviously found that the geometrical parameters of the S_6 hexaadduct are very similar to those of D_3 hexaadduct. The bond lengths of C4−C5 and C5−C6 are 1.611 and 1.528 Å, respectively, which are 0.216 and 0.074 Å, respectively, larger than that of the parent C_{60}. The angle of C4−C5−C6 decreases by 7.1° from 120.0° of the parent C_{60} to 113.9°, whereas the angle of C5−C6−C7 increases from 108.0 to 110.4°. The dihedral angles of C1−C2−C3−C4 and C2−C3−C4−C5 are 13.2 and −10.3°, respectively.

Compared with the experimental values of T_h and D_3 hexapyrrolidine,[9] the geometrical parameters of the D_3 structure in this work are in agreement with the experimental ones. For the T_h structure, the large difference is that the pentagon rings of the functionalized group have no planar property in the experimental results. The methyl groups in the functionalized group are replaced by hydrogen atoms in this work in order to reduce the calculation load, and there is a long distance between the two neighboring hydrogen atoms in the two neighboring functional groups (5.966 Å), which results in the decrease of steric hindrance and electrostatic interaction in the T_h structure. This may be the reason resulting in the difference from the experimental ones.

(2) Spectrum Properties of the Hexapyrrolidine Fullerene C_{60} Derivatives. The electronic transition energies and oscillator strengths are calculated at the TDB3LYP/6-31G* level. The absorption process occurs principally by electronic transition from the ground singlet state S_0 to the low excitation singlet states S_n. On the other hand, the fluorescent emission occurs from the excited states S_n to S_0. Therefore, the excited singlet states are responsible for the fluorescent process.

Table 2 lists the transition energies and oscillator strengths from S_0 to S_n. For the T_h hexaadduct, the transition energy from S_0 to S_1 is 2.5104 eV, which is generated by the promotion of one electron from the highest occupied molecular orbital

TABLE 2: HOMO−LUMO Gaps and the Transition Energies and Oscillator Strengths (the Values Are in Parentheses) from S_0 to S_n

	T_h	D_3	S_6	C_{60}
HOMO−LUMO gaps (eV)	3.1897	3.1557	2.5938	2.7693
$S_0 \rightarrow S_1$ (eV)	2.5104 (0.0000)	2.5635 (0.0051)	1.9331 (0.0000)	2.1035 (0.0000)
$S_0 \rightarrow S_2$ (eV)	2.6083 (0.0000)	2.6483 (0.0052)	1.9479 (0.0000)	2.1153 (0.0000)
$S_0 \rightarrow S_3$ (eV)	2.6189 (0.0000)	2.8804 (0.0000)	1.9602 (0.0000)	2.2874 (0.0000)
$S_0 \rightarrow S_4$ (eV)	2.7469 (0.0000)	2.8894 (0.0055)	2.0984 (0.0000)	3.2212 (0.0000)
$S_0 \rightarrow S_5$ (eV)	2.8250 (0.0000)	2.9178 (0.0466)	2.5530 (0.0000)	3.2398 (0.0000)
$S_0 \rightarrow S_6$ (eV)	2.8682 (0.0005)	2.9813 (0.0000)	2.6418 (0.0000)	3.2930 (0.0000)
$S_0 \rightarrow S_7$ (eV)	2.9649 (0.0083)	3.0458 (0.0171)	2.7688 (0.0066)	3.4409 (0.0000)

(HOMO) to the lowest unoccupied molecular orbital (LUMO). Due to the HOMO belonging to e_u symmetry and the LUMO belonging to e_g symmetry, such electronic transition is forbidden. This is the reason the calculated oscillator strength of the S_1 state is zero. However, the electron transition from S_0 to S_6 is mainly contributed from the configuration of MO_{245} (belonging to t_u symmetry) to MO_{253} (belonging to e_g symmetry), so that this transition is allowed. The calculated oscillator strength of the S_6 state is 0.0005. The absorption peak of maximum wavelength occurs at 432 nm, which corresponds to the transition from S_0 to S_6. As for the D_3 hexaadduct, the transition energy from S_0 to S_1 is 2.5635 eV. Its first singlet excited state S_1 is also generated by the promotion of one electron from the HOMO (MO_{252}) to the LUMO (MO_{253}). MO_{252} and MO_{253} belong to a_1 and a_2 symmetry, respectively, so that such electronic transition is allowed. The obtained oscillator strength is 0.0051. Thus, the absorption peak of maximum wavelength occurs at 484 nm, which corresponds to the transition from S_0 to S_1. Finally, the S_6 hexaadduct of which the transition energy from S_0 to S_1 is 1.9331 eV is also studied. Both the HOMO (MO_{251}, MO_{252}) and the LUMO (MO_{253}, MO_{254}) are 2-fold degenerate. Due to the constraint of transition selection rules, the electronic transitions from S_0 to S_n ($n = 1-6$) are forbidden. The maximum wavelength peak occurs at 448 nm, which corresponds to the transition from S_0 to S_7.

From the above analyses and the values listed in Table 2, we can find that the transition energies from S_0 to S_1 of the T_h hexaadduct and the D_3 hexaadduct have a remarkable blue shift by comparison with that of the C_{60} parent.[22] These shift trends are in an agreement with experimental ones,[9] although our calculated results are under ideal conditions of an isolated molecule and do not consider the contribution of vibration transitions. However, the first singlet excitation energy of the S_6 hexaadduct has a red shift compared with that of C_{60}. Finally, we also can predict that the fluorescent peak of minimum wavelength will be larger than 494 nm for the T_h hexaadduct and 484 for the D_3 hexaadduct according to Kasha's rules and Stoke's law. The obtained results match well with the experimental ones.[9] However, the fluorescent peak of minimum wavelength for the S_6 hexaadduct may be larger than 641 nm, because its transition energy from S_1 to S_0 is 1.9331 eV. In view of this result, we can find that the different positions located by six addends may result in the different spectrum properties.

(3) Third-Order Polarizabilities of the Three Optical Processes THG, EFISHG, and DFWM. Before attempting to compute the variation of the third-order polarizability versus wavelength, it is necessary to investigate the convergent behavior in the summation of excited states and to determine whether the results calculated from the TDB3LYP method are reliable for these chosen compounds. Figure 2 shows the plots of the calculated third-order polarizabilities, γ, of the T_h, D_3, and S_6 hexaadducts for the DFWM optical process in the static case. It can be found that the convergences are stable after summation over about 50 states for the T_h hexaadduct and the D_3 hexaadduct. However, it is a pity that the S_6 hexaadduct has no good convergence. To ensure that the result is reliable, we employ a small basis set (3-21G*) to calculate 70 excited states for the S_6 hexaadduct. The computational result indicates that the states after 50 have no large contribution to the third-order polarizability of the S_6 hexaadduct. Accordingly, it is a reasonable approximation in the calculation of γ by employing 50 states in the SOS method in this work.

Figure 3 depicts the calculated dynamic $\langle\gamma\rangle$ with different optical physical processes from frequency 0.0 to 1.0 eV/$\hbar$ at the ground state for the T_h, D_3, and S_6 hexaadducts. In the static case where the input photon energy is zero, the values of all three processes, THG, EFISHG, and DFWM, are the same for each molecule. The values for the T_h, D_3, and S_6 hexaadducts are respectively 0.16×10^{-34}, 0.20×10^{-34}, and 0.17×10^{-34} esu. Furthermore, in the dynamic case when the input energy is 0.800 eV, $\langle\gamma(\omega)\rangle$, $\langle\gamma(2\omega)\rangle$, and $\langle\gamma(3\omega)\rangle$ are respectively 0.21×10^{-34}, 0.25×10^{-34}, and 0.51×10^{-34} esu for the T_h hexaadduct; 0.27×10^{-34}, 0.34×10^{-34}, and 0.84×10^{-34} esu for the D_3 hexaadduct; and 0.24×10^{-34}, 0.30×10^{-34}, and 1.00×10^{-34} esu for the S_6 hexaadduct.

In eq 1, we can see that the value of polarizability comes from the summations of type-I and type-II terms, and both the terms are governed by the product of the transition dipole moments and the transition energies. The type-I and type-II terms are the competing third-order virtual excitation processes, and the electron transitions between two states in each term are allowed for the dipole selection rules. Figure 4 shows the third-order virtual excitation processes of types I and II. For the type-I process, S_0 is the ground state, and S_l and S_m are one-photon allowed excited states. The intermediate state is S_0 itself, and this process makes a negative contribution to γ at a low frequency region. For the T_h, D_3, and S_6 hexaadducts, the calculated values of $\langle\gamma(0)\rangle_I$ are -0.004×10^{-34}, -0.05×10^{-34}, and -0.02×10^{-34} esu in the static case, and the calculated dynamic values of $\langle\gamma(\omega)\rangle_I$ in the DFWM process are -0.005×10^{-34}, -0.06×10^{-34}, and -0.02×10^{-34} esu at an input photon energy of 0.800 eV.

For the type-II process in Figure 4, the intermediate state S_j is a two-photon allowed excited state. The calculated values of

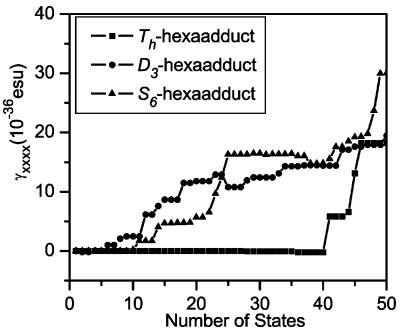

Figure 2. Convergent behavior of third-order polarizability.

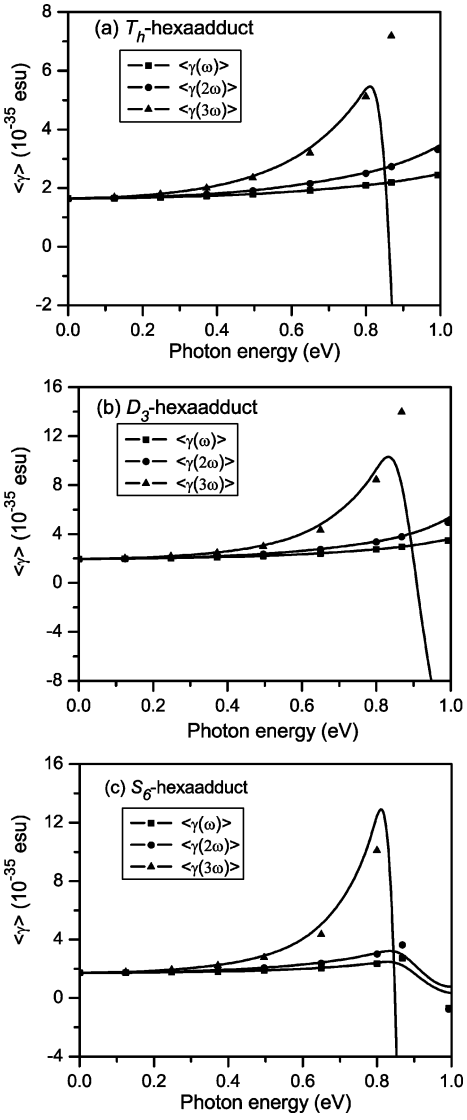

Figure 3. Calculated dispersion behavior of $\langle\gamma\rangle$ of THG, EFISHG, and DFWM at the ground state.

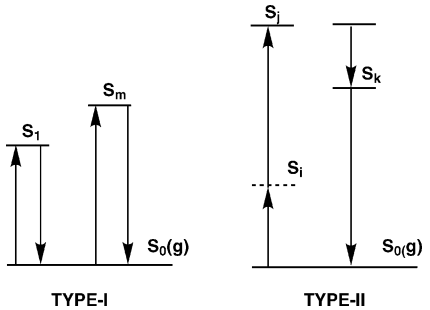

Figure 4. Two virtual excitation processes for third-order polarizability.

$\langle\gamma(0)\rangle_{II}$ are 0.17×10^{-34}, 0.24×10^{-34}, and 0.19×10^{-34} esu in the static case, and the calculated dynamic values of $\langle\gamma(\omega)\rangle_{II}$ in the DFWM process are 0.21×10^{-34}, 0.33×10^{-34}, and 0.26×10^{-34} esu at an input photon energy of 0.800 eV for the T_h, D_3, and S_6 hexaadducts, respectively. Accordingly, the type-II process makes a larger positive contribution to γ and makes the overall sign positive for the T_h, D_3, and S_6 hexaadducts.

(4) Two-Photon Absorption Cross Sections. The calculated frequency-dependent TPA cross sections, $\delta(\omega)$, of the investigated compounds are plotted in Figure 5 from incident energies of 1.40−2.00 eV. It is found that the largest average value of

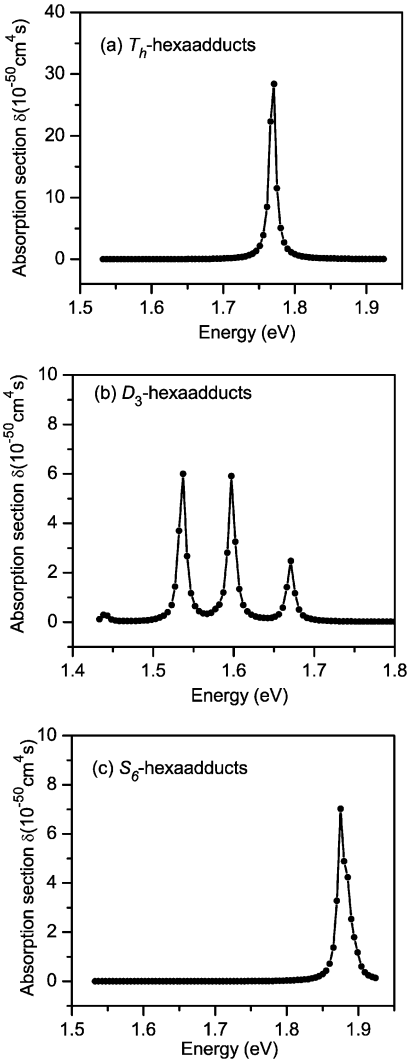

Figure 5. Calculated frequency-dependent two-photon absorption cross section.

resonant TPA, $\langle\delta\rangle$, of the D_3 hexaadduct has a red shift compared with those of the T_h and S_6 hexaadducts. The largest $\langle\delta\rangle$ value of the D_3 hexaadduct is localized at ∼1.537 eV, and those of the T_h and S_6 hexaadducts are localized at ∼1.771 and ∼1.875 eV, respectively.

Furthermore, we will search for the origin of large TPA cross section, $\delta(\omega)$, of the T_h, D_3, and S_6 hexaadducts. From eq 3, it can be found that the $\delta(\omega)$ value only depends on the imaginary part of third-order polarizability $Im\gamma(-\omega; \omega, \omega, -\omega)$, while the input frequency is given at the vacuum medium. Accordingly, the two-photon states contributing to $Im\gamma(-\omega; \omega, \omega, -\omega)$ shown in eq 4 are also the contributions to the $\delta(\omega)$ value. Figure 6 presents the plots of $Im\gamma(-\omega; \omega, \omega, -\omega)$ values (related to the TPA cross section of δ_a) versus two-photon states at the characteristic wavelength (resonant wavelength). It can be seen from Figure 6 that the resonant TPA cross sections of the T_h, D_3, and S_6 hexaadducts are all contributed from one two-photon state. For the T_h hexaadduct, one electron is promoted from the ground state to state 41 by absorbing two-photon energy, and the transition energy from the ground state to state 41 (3.5375 eV) is equal to the two-photon energy (2×1.771 eV), which makes two-photon resonance absorption. The two-photon state 41 has the greatest contribution from the configurations $MO_{245} \rightarrow MO_{255}$, $MO_{246} \rightarrow MO_{256}$, and $MO_{247} \rightarrow MO_{257}$. For the D_3 hexaadduct, one electron is promoted from the ground state to

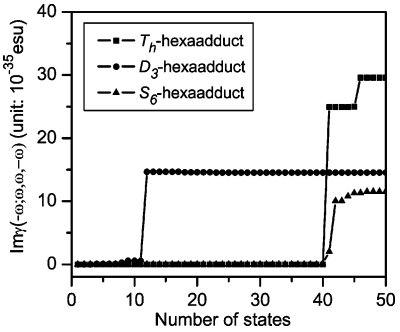

Figure 6. Plots of $Im\gamma(-\omega; \omega, \omega, -\omega)$ values vs two-photon states at the resonant wavelength.

state 12 by absorbing two-photon energy, and the transition energy from the ground state to state 12 (3.0730 eV) is equal to the two-photon energy (2×1.537 eV), which makes two-photon resonance absorption. The two-photon state 12 has the greatest contribution from the configurations $MO_{248} \rightarrow MO_{254}$ and $MO_{249} \rightarrow MO_{255}$. For the D_3 hexaadduct, the electron transition from the ground state to state 42 makes two-photon resonance absorption, and the transition energy from the ground state to state 42 (3.7501 eV) is equal to two-photon energy (2×1.875 eV). The two-photon state 42 has the greatest contribution from the configuration $MO_{243} \rightarrow MO_{255}$.

By analyses of the molecular orbital components resulting in two-photon absorption, it can be seen that the occupied molecular orbitals (MO_{245}, MO_{246}, and MO_{247} of the T_h hexaadduct, MO_{248} and MO_{249} of the D_3 hexaadduct, and MO_{243} of the S_6 hexaadduct) are mostly composed of atomic orbits of functionalized groups, whereas the virtual orbitals (MO_{255}, MO_{256}, and MO_{257} of the T_h hexaadduct, MO_{254} and MO_{255} of the D_3 hexaadduct, and MO_{255} of the S_6 hexaadduct) are composed of atomic orbitals of the C_{60} cage. Obviously, the two-photon absorptions of the T_h, D_3, and S_6 hexaadducts all originate from the electronic transitions from functionalized groups to the C_{60} cage.

IV. Conclusions

Using the B3LYP method at the 6-31G* level, the equilibrium geometries of three isomeric hexapyrrolidine C_{60} derivatives with T_h, D_3, and S_6 symmetries have been optimized, and the results show that the geometrical parameters in the vicinity of the functionalized group have remarkable changes by comparison with the ones of the parent C_{60}. The excited state properties and third-order nonlinear optical polarizabilities, γ, in the different optical processes of THG, EFISHG, and DFWM have been calculated by using the TDB3LYP model at the 6-31G* level coupled with the sum-over-states method. The calculated results indicate that the transition energies from S_0 to S_1 of the T_h hexaadduct and the D_3 hexaadduct have a remarkable blue shift by comparison with that of the C_{60} parent. These results are in good agreement with the experimental ones. However, the first singlet excitation energy of the S_6 hexaadduct has a red shift compared with that of the C_{60} parent. This result indicates that the different positions located by six addends may result in the different spectrum properties. Finally, the two-photon absorption cross sections have also been calculated by using the relation between the imaginary part of third-order polarizability and cross section. It is found that the largest average value of resonant TPA, $\langle\delta\rangle$, of the D_3 hexaadduct has a red shift compared with those of the T_h and S_6 hexaadducts.

Acknowledgment. This investigation was based on work supported by the National Natural Science Foundation of China under project 20373073, the Science Foundation of the Fujian Province (no. E0210028 and no. 2002F010), and the Foundation of State Key Laboratory of Structural Chemistry (no. 030060).

References and Notes

(1) Taylor, R.; Walton, D. R. M. *Nature* **1993**, *363*, 685.
(2) Diederich, F.; Thilgen, C. *Science* **1996**, *271*, 317.
(3) Sun, Y.-P.; Lawson, G. E.; Riggs, J. E.; Ma, B.; Wang, N.; Moton, D. K. *J. Phys. Chem. A* **1998**, *102*, 5520.
(4) Sun, Y.-P.; Guduru, R.; Lawson, G. E.; Mullins, J. E.; Guo, Z.; Quinlan, J.; Bunker, C. E.; Gord, J. R. *J. Phys. Chem. B* **2000**, *104*, 4652.
(5) Coheur, P.-F.; Cornil, J.; dos Santos, D. A.; Birkett, P. R.; Liévin, J.; Brédas, J. L.; Walton, D. R. M.; Taylor, R.; Kroto, H. W.; Colin, R. *J. Chem. Phys.* **2000**, *112*, 8555.
(6) Coheur, P.-F.; Cornil, J.; dos Santos, D. A.; Birkett, P. R.; Liévin, J.; Brédas, J. L.; Janot, J.-M.; Seta, P.; Leach, S.; Walton, D. R. M.; Taylor, R.; Kroto, H. W.; Colin, R. *Synth. Met*. **1999**, *103*, 2407.
(7) Levitus, M.; Schick, G.; Lunkwitz, R.; Rubin, Y.; Garcia-Garibay, M. A. *J. Photochem. Photobiol., A* **1999**, *127*, 13.
(8) Luo, C.; Fujitsuka, M.; Watanabe, A.; Ito, O.; Gan, L.; Huang, Y.; Huang, C.-H. *J. Chem. Soc., Faraday Trans.* **1998**, *94*, 527.
(9) Schick, G.; Levitus, M., Kvetko, L.; Johnson, B. A.; Lamparth, I.; Lunkwitz, R.; Ma, B.; Khan, S. I.; Garcia-Garibay, M. A.; Rubin, Y. *J. Am. Chem. Soc.* **1999**, *121*, 3246.
(10) Hutchison, K.; Gao, J.; Schick, G.; Rubin, Y.; Wudl, F. *J. Am. Chem. Soc.* **1999**, *121*, 5611.
(11) Frisch, M. J.; et al. *GAUSSIAN98*; Gaussian Inc.: Pittsburgh, PA, 1998.
(12) Becke, A. D. *J. Chem. Phys.* **1993**, *98*, 5648.
(13) Hirsch, A.; Lamparth, I.; Grösser, T.; Karfunkel, H. R. *J. Am. Chem. Soc.* **1994**, *116*, 9385.
(14) Stratmann, R. E.; Scuseria, G. E.; Frisch, M. J. *J. Chem. Phys.* **1998,** *109*, 8218.
(15) Bauemschmitt, R.; Ahlrichs, R. *Chem. Phys. Lett.* **1996**, *256*, 454.
(16) Casida, M. E.; Jamorski, C.; Casida, K. C.; Salahub, D. R. *J. Chem. Phys*. **1998**, *108*, 4439.
(17) Orr, B. J.; Ward, J. F. *Mol. Phys.* **1971**, *20*, 513.
(18) Pierce, B. M. *J. Chem. Phys.* **1989**, *91*, 791.
(19) Bredas, J. L.; Adant, C.; Tackx, P.; Persoons, A.; Pierce, B. M. *Chem. Rev.* **1994**, *94*, 243.
(20) Dick, B.; Hochstrasser, R. M.; Trommsdorff, H. P. *Nonlinear Optical Properties of Organic Molecules and Crystals*; Chemla, D. S., Zyss, J., Eds.; Academic Press: Orlando, FL, 1987; Vol. 2, pp 167−170.
(21) Atkins, P. W. *Molecular Quantum Mechanics*, 2nd ed.; Oxford University Press: 1983; Chaper 11.
(22) Li, X.-D.; Cheng, W.-D.; Wu, D.-S.; Zhang, H.; Gong, Y.-J.; Lan, Y.-Z. *Chem. Phys. Lett*. **2003**, *380*, 480.